Low-order longitudinal modes of single-component plasmas

M. D. Tinkle,[a] R. G. Greaves, and C. M. Surko
Department of Physics, University of California, San Diego, La Jolla, California 92093-0319

(Received 31 October 1994; accepted 21 April 1995)

The low-order modes of spheroidal, pure electron plasmas have been studied experimentally, both in a cylindrical electrode structure and in a quadrupole trap. Comparison is made between measurements of mode frequencies, recent analytical theories, and numerical simulations. Effects considered include trap anharmonicity, image charges, and temperature. Quantitative agreement is obtained between the predictions and these measurements for spheroidal plasmas in the quadrupole trap. In many experiments on single-component plasmas, including antimatter plasmas, the standard diagnostic techniques used to measure the density and temperature are not appropriate. A new method is presented for determining the size, shape, average density, and temperature of a plasma confined in a Penning trap from measurements of the mode frequencies. © *1995 American Institute of Physics.*

I. INTRODUCTION

Single-component plasmas have been extensively studied, both experimentally and theoretically.[1,2] Most experimental studies are conducted in cylindrically symmetric Penning traps, in which radial confinement is provided by a magnetic field and axial confinement is provided by an externally imposed electrostatic potential well. Pure electron plasmas have typically been studied in traps with long cylindrical electrodes[3] to increase the total number of trapped particles and to reduce the importance of end effects, which are difficult to treat theoretically. On the other hand, ion plasmas and small numbers of ions that are not in a plasma state are usually studied in short traps with precision hyperboloidal electrodes.[4]

Experiments with pure ion plasmas in precision quadrupole traps have begun to combine these two different fields of Penning trap research.[4] Although the number of particles trapped in these experiments is still small ($\simeq 10^5$), laser cooling lowers their temperature sufficiently to make them plasmas. In some experiments,[4] the temperature is so low ($T < 10$ mK) that the plasmas become strongly coupled, forming concentric shells.[5] Because a quadrupole trap is used, the plasmas are spheroidal,[6] rather than cylindrical. Remarkably, an exact theory exists[7] for the normal modes of these plasmas, in the limit of very low temperatures. Some of the predicted modes have been observed at frequencies in very good agreement with the theory.[8,9]

The experiments described in this paper were performed with large numbers of particles (10^7–10^9) in an approximate quadrupole trap. Single-component plasmas of various species have been studied in the same trap, including pure electron, pure ion, and pure positron plasmas. In an earlier paper, we presented results for modes in pure electron plasmas.[10] In this paper we describe the experiments in more detail, and also present the first data on collective plasma modes in a pure positron plasma. These experiments have led to an improved understanding of the temperature and shape dependence of the plasma mode frequencies in these plasmas, with the prospect of their application as a diagnostic in a variety of experiments.[10,11] Other experiments with positron plasmas and pure ion plasmas are discussed elsewhere.[12,13]

The trap used in the experiments described here was designed to accumulate and store positrons.[14,15] There are a variety of applications for trapped positrons including plasma physics applications, such as the study of electron–positron plasmas,[16–20] and tokamak transport experiments.[21] Other applications include the search for resonant states in electron–positron scattering experiments,[22] positron annihilation studies,[23–27] the production of low-emittance positron beams,[28] and the formation of antihydrogen.[29]

The plasma mode studies reported here were begun with the intention of developing a nonperturbative diagnostic of the properties of a positron plasma, for which neither the probes used for neutral plasmas nor the destructive diagnostics used for electron plasmas are desirable. The same techniques could also be used to monitor antiproton plasmas[30,31] or as an adjunct to the usual techniques for electron plasma experiments. The properties of positron plasmas are the same as those of electron plasmas, except that positron confinement is dominated by annihilation on neutral gas molecules in our trap. Because electrons are more convenient to work with, positrons were not used for most of the mode studies described here.

The plasmas are formed by trapping particles from a weak beam, using collisions with a neutral buffer gas to remove the required energy. As a result, the plasmas cool to room temperature, but they may be heated to about 0.5 eV by the application of RF noise. Using standard techniques, the temperature and the radial density profile can be measured. Several of the normal modes predicted by Dubin[7] are ob-

[a]Present address: Plasma Physics Laboratory, Columbia University, New York, New York 10027.

 1070-664X/95/2(8)/2880/15/$6.00 © 1995 American Institute of Physics

Downloaded 21 Jun 2001 to 132.239.73.116. Redistribution subject to AIP license or copyright, see http://ojps.aip.org/pop/popcr.jsp

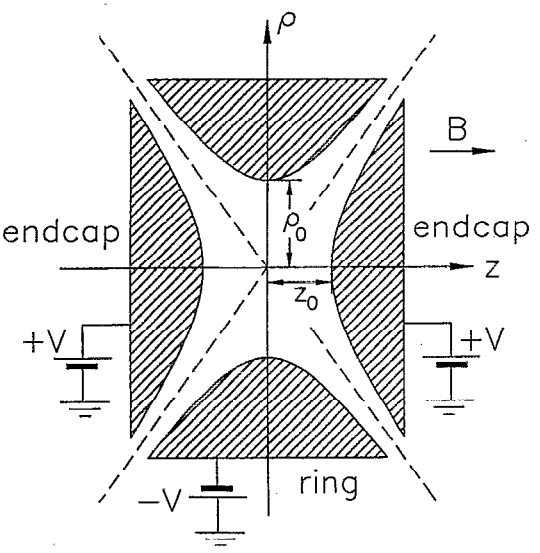

FIG. 1. Cross section of a quadrupole Penning trap. The trap is cylindrically symmetric about the z axis.

served, although not always at exactly the frequencies predicted by the cold fluid theory. The discrepancies are mostly the result of the plasma temperature, and the data are in excellent agreement with numerical simulations of the plasmas.[10]

This paper is organized in the following manner. In Sec. II we describe the theory of single-component plasmas in quadrupole traps. The experimental equipment and techniques used are described in Sec. III. The results obtained with electron plasmas are presented in Sec. IV and compared with the cold fluid theory and with numerical simulations. The use of these results as diagnostics is also described, and data obtained with positron plasmas are presented. Section V, which concludes the paper, is a brief summary of the present state of knowledge in this area.

II. THEORY

A. Plasma equilibrium

The electrodes of an ideal quadrupole Penning trap, shown in Fig. 1, are hyperboloids of revolution with their axis of symmetry (defined as the z axis) aligned with a uniform magnetic field, B, and sharing the asymptotes $\rho = \pm\sqrt{2}z$, where $\rho = \sqrt{x^2+y^2}$ is the cylindrical radius coordinate. Various choices for the hyperboloids are possible. The standard one is the asymptotically symmetric Penning trap, in which the electrode surfaces satisfy the equation

$$z^2-\tfrac{1}{2}\rho^2=\pm z_0^2. \tag{1}$$

The minimum distance from the trap center to either of the two "endcap" electrodes (described by the plus sign in the above equation) is thus z_0, and the distance to the "ring" electrode (described by the minus sign) is $\rho_0=\sqrt{2}z_0$. If the endcaps and the ring are set to potentials V and $-V$, respectively, the electric potential has the form

$$\Phi(\rho,z)=\frac{V}{z_0^2}\left(z^2-\frac{1}{2}\rho^2\right).$$

In the absence of the electric field of the trap, a charged particle would move freely in the z direction, while executing circular motions in x and y at the cyclotron frequency, $\Omega_c=qB/mc$, where c is the speed of light, and q and m are the charge and mass of the particle, respectively. A charged particle confined in the trap electric field follows a more complicated path that is the superposition of three independent harmonic oscillations. In the z direction, it oscillates about the origin at a frequency, $\omega_z = \sqrt{2qV/mz_0^2}$. Its motion in the x and y coordinates consists of a rapid circular motion downshifted from the cyclotron frequency:

$$\Omega_c'=\frac{\Omega_c}{2}+\frac{1}{2}\sqrt{\Omega_c^2-2\omega_z^2}, \tag{2}$$

accompanied by a slower circular drift around the z axis at the magnetron frequency,

$$\Omega_M=\frac{\Omega_c}{2}-\frac{1}{2}\sqrt{\Omega_c^2-2\omega_z^2}. \tag{3}$$

These two frequencies are the roots, Ω, of the equation

$$\omega_z^2=2\Omega(\Omega_c-\Omega). \tag{4}$$

When $\Omega_c' \gg \Omega_M$ and the electric field varies slowly over the radius of the cyclotron orbits, conditions that are well satisfied in most electron plasma experiments, the magnetron motion may be thought of as the $\mathbf{E}\times\mathbf{B}$ drift of the guiding center of the particle. The amplitudes and phases of the three independent oscillations may be determined from the initial conditions. Typically, the amplitudes are of more interest than the phases, since they are constants of the motion. In particular, the radius of the cyclotron motion is

$$\rho_c=\left(\frac{\dot\rho^2+\rho^2(\dot\phi+\Omega_M)^2}{\Omega_c^2-2\omega_z^2}\right)^{1/2},$$

where ρ is the radial position and $\dot\rho$ and $\rho\dot\phi$ are the radial and azimuthal components of the particle velocity. The radius, ρ_d, of the magnetron drift motion is found from the same formula by replacing Ω_M with Ω_c'.

The thermal equilibrium of a large number of particles confined in a cylindrical Penning trap at a low temperature is a uniform-density cylindrical plasma, rotating rigidly.[32] The rotation frequency, ω_r, may be either of the two roots of the equation

$$\omega_p^2=2\omega_r(\Omega_c-\omega_r), \tag{5}$$

where $\omega_p=(4\pi q^2 n/m)^{1/2}$ is the plasma frequency and n is the number density of the plasma. Surprisingly, this equation also applies to the low-temperature equilibria of plasmas in quadrupole traps, which are uniform-density, rigidly rotating spheroids.[6] The spheroids are biaxial ellipsoids with rotational symmetry about the z axis, so they are completely specified by their length, L, along the z axis and their radius, r_p, at $z=0$. The ratio of length to diameter,

Downloaded 21 Jun 2001 to 132.239.73.116. Redistribution subject to AIP license or copyright, see http://ojps.aip.org/pop/popcr.jsp

$$\alpha=\frac{L}{2r_p},$$

is referred to as the aspect ratio. In equilibrium, α is related to the plasma density by the equation[33]

$$\omega_p^2=\omega_z^2\frac{2}{A_3(\alpha)}, \tag{6}$$

where

$$A_3(\alpha)=\frac{2Q_1^0[\alpha(\alpha^2-1)^{-1/2}]}{\alpha^2-1}, \tag{7}$$

and Q_1^0 is a Legendre function of the second kind. As shown in Fig. 2, ω_p is a monotonically increasing function of α that approaches its minimum value, $\omega_p=\omega_z$, as $\alpha\to 0$. This implies that $\omega_r\geq\Omega_M$, as may be seen from a comparison of Eq. (4) and Eq. (5).

B. Plasma oscillations

The dispersion relation for the normal modes of these non-neutral plasma spheroids has been derived in the cold fluid limit by Dubin,[7] using spheroidal coordinates and a clever frequency-dependent coordinate transformation to match solutions for the potential perturbation, $\delta\Phi$, at the plasma surface. This is the first analytical theory to treat the boundary conditions of a finite plasma exactly.

To understand the structure of the normal modes described by the theory requires some discussion of the coordinate systems used. Outside the plasma, spheroidal coordinates (ξ_1,ξ_2,ϕ) are used. The azimuthal angle, ϕ, is the same as in cylindrical coordinates, and ξ_1 and ξ_2 are related to cylindrical coordinates by the equations

$$\rho=[(\xi_1^2-d^2)(1-\xi_2^2)]^{1/2},$$

$$z=\xi_1\xi_2.$$

With the parameter d chosen as $d^2=(L/2)^2-r_p^2$, the plasma surface is described by $\xi_1=L/2$. The solutions to Laplace's equation can be expanded in terms of the associated Legendre functions as

$$\delta\Phi^o(\xi_1,\xi_2,\phi,t)=\sum_{l=1}^{\infty}\sum_{m=-l}^{l}\delta\Phi^o_{l,m}(\xi_1,\xi_2,\phi,t),$$

$$\delta\Phi^o_{l,m}(\xi_1,\xi_2,\phi,t)=A_{l,m}Q_l^m(\xi_1/d)P_l^m(\xi_2)e^{i(m\phi-\omega t)},$$

where the $A_{l,m}$ are constant coefficients.

Inside the plasma, a different set of spheroidal coordinates, $(\bar{\xi}_1,\bar{\xi}_2,\phi)$, is used in which the relation to the z coordinate is altered:

$$\rho=[(\bar{\xi}_1^2-\bar{d}^2)(1-\bar{\xi}_2^2)]^{1/2},$$

$$z=(\epsilon_3/\epsilon_1)^{1/2}\bar{\xi}_1\bar{\xi}_2,$$

where

$$\bar{d}^2=\left(\frac{L}{2}\right)^2\frac{\epsilon_1}{\epsilon_3}-r_p^2. \tag{8}$$

The quantities ϵ_1 and ϵ_3 are elements of the dielectric tensor appropriate to a single-component plasma in a uniform magnetic field,

$$\epsilon=\begin{bmatrix}\epsilon_1 & -i\epsilon_2 & 0\\ i\epsilon_2 & \epsilon_1 & 0\\ 0 & 0 & \epsilon_3\end{bmatrix}, \tag{9}$$

and are related to the plasma parameters as follows:

$$\epsilon_1=1-\omega_p^2/(\omega^2-\Omega_v^2),$$

$$\epsilon_2=\Omega_v\omega_p^2/\omega(\omega^2-\Omega_v^2),$$

$$\epsilon_3=1-\omega_p^2/\omega^2,$$

where $\Omega_v=\Omega_c-2\omega_r$. In this coordinate system, the surface of the plasma is described by $\bar{\xi}_1=(\epsilon_1/\epsilon_3)^{1/2}L/2$, the Poisson's equation is transformed into Laplace's equation. As a result, the perturbed potential inside the plasma may be written as

$$\delta\Phi^i(\bar{\xi}_1,\bar{\xi}_2,\phi,t)=\sum_{l=1}^{\infty}\sum_{m=-l}^{l}\delta\Phi^i_{l,m}(\bar{\xi}_1,\bar{\xi}_2,\phi,t),$$

$$\delta\Phi^i_{l,m}(\bar{\xi}_1,\bar{\xi}_2,\phi,t)=B_{l,m}P_l^m(\bar{\xi}_1/\bar{d})P_l^m(\bar{\xi}_2)e^{i(m\phi-\omega t)}.$$

Matching $\delta\Phi^i_{l,m}$ and $\delta\Phi^o_{l,m}$ at the surface leads to the dispersion relation

$$\epsilon_3+m\alpha\left(\alpha^2-\frac{\epsilon_3}{\epsilon_1}\right)^{1/2}\frac{P_l^m(k_1)}{P_l^{m'}(k_1)}=\left(\frac{\alpha^2-\epsilon_3/\epsilon_1}{\alpha^2-1}\right)^{1/2}\frac{P_l^m(k_1)Q_l^{m'}(k_2)}{P_l^{m'}(k_1)Q_l^m(k_2)}, \tag{10}$$

where $k_1=\alpha/(\alpha^2-\epsilon_3/\epsilon_1)^{1/2}$, $k_2=\alpha(\alpha^2-1)^{-1/2}$, and the primes indicate derivatives taken with respect to the entire argument.

For strongly magnetized plasmas, in which $\Omega_c\gg\omega_p$ and $\Omega_c\gg\omega_z$, the dispersion relation for low-frequency eigenmodes with azimuthal symmetry (i.e., $m=0$) reduces to

$$1-\frac{\omega_p^2}{\omega^2}=\left(\frac{\alpha^2-1+\omega_p^2/\omega^2}{\alpha^2-1}\right)^{1/2}\frac{P_l(k_1)Q_l^{0'}(k_2)}{P_l'(k_1)Q_l^0(k_2)}, \tag{11}$$

and k_1 simplifies to $k_1=\alpha(\alpha^2-1+\omega_p^2/\omega^2)^{-1/2}$. When scaled by ω_z, the normal mode frequencies are functions of α only, as shown in Fig. 2 for several of the lowest-order modes. Sketches of fluid motions during one phase of the oscillation are included in Fig. 2 to indicate the spatial structure of the modes. The modes shown in this figure with no radial structure are the Trivelpiece–Gould modes[34] for spheroidal plasmas. The Appendix includes a discussion of the solution of Eq. (11).

Another set of modes of interest are the purely azimuthal modes, for which $l=|m|$. In this paper we deal only with axial modes of electron and pure positron plasmas. We have discovered that the azimuthal modes of pure ion plasmas can be investigated in a novel steady-state mode of operation of our trap, and the results are to be published in a separate paper.[13] However, both families of modes can be investigated in either pure electron or pure ion plasmas.

Downloaded 21 Jun 2001 to 132.239.73.116. Redistribution subject to AIP license or copyright, see http://ojps.aip.org/pop/popcr.jsp

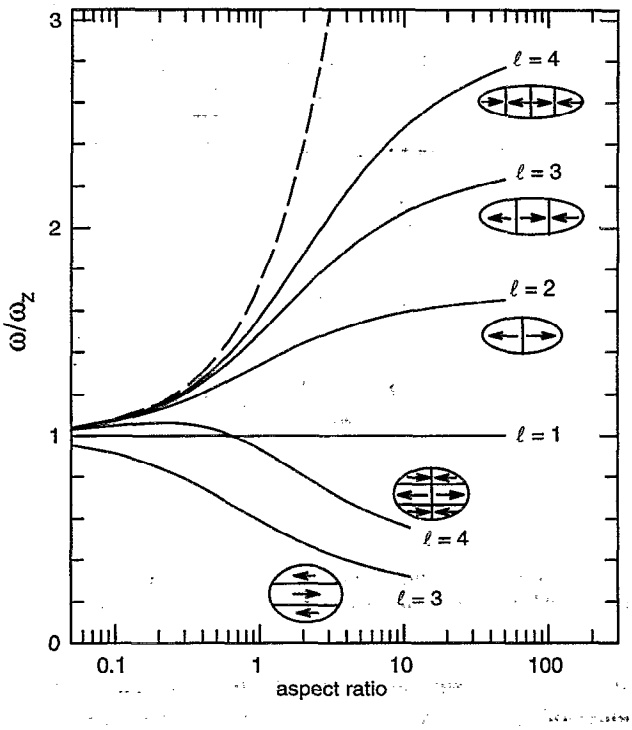

FIG. 2. Cold fluid theory for axial modes of highly magnetized spheroidal plasmas: frequency as a function of aspect ratio for several low-order modes, scaled by ω_z. The dashed line is the plasma frequency.

C. Thermal effects

The cold fluid equilibrium described above is valid if the Debye shielding length, $\lambda_D=(k_BT/4\pi nq^2)^{1/2}$, is much smaller than the size of the plasma, i.e., $\lambda_D \ll L, r_p$. Here T is the plasma temperature and k_B is the Boltzmann constant. In this case, the thermal equilibrium deviates from a uniform-density spheroid only at the edge, where the density falls to zero in a distance of a few Debye lengths. The plasma pressure causes the equilibrium spheroid to elongate slightly along the magnetic field. In the opposite limit, $\lambda_D \gg L, r_p$, the particle interactions are negligible compared to their thermal energy and the trap potential, and their distribution in z is a Gaussian, with $\langle z^2\rangle = k_BT/m\omega_z^2$.

The cold fluid mode theory requires $\lambda_D \ll L, r_p$, but, in addition, λ_D must be much smaller than the wavelength, λ, of the mode being considered. If this is not the case, the frequency of compressional plasma modes would be expected to increase due to the plasma pressure, and Landau damping will become important. As a result, even "cool" plasmas will show only a finite number of modes, and the most robust will be the lowest-order modes, which have the longest wavelengths. It is possible to estimate the effects of plasma temperature on the mode frequencies to first order in T,[33,35] as described in Sec. IV B 3. A warm fluid theory in which a pressure term is added to the fluid equation of motion is quite successful for low enough T, but is confounded by the occurrence of nonphysical acoustic modes for higher temperatures.[36]

Three of the global modes in the cold fluid theory are not truly plasma modes, but merely motions of the plasma center of mass. These modes, namely the axial bounce, cyclotron, and magnetron modes, should have frequencies independent of the plasma size, shape, and temperature in a perfect quadrupole trap, as long as image charges may be neglected.

D. Image charges

Because the plasmas studied are not always small in either total charge or spatial scale, the effects of the charges drawn onto the electrodes to maintain constant potentials in the presence of the plasma (referred to as the plasma "image charge") are not always negligible. The attractive interaction between the plasma and its image charge modifies the effective trap potential from that of a perfect quadrupole, making the equilibrium nonspheroidal and complicating the prediction of mode frequencies. For a small plasma, however, the dominant effect of the image charge is to change the strength of the quadrupole potential to an extent proportional to the plasma charge, with a constant of proportionality dependent on the geometry of the trap electrodes. A number of papers have treated the problem of image charge effects in quadratic wells. Wineland and Dehmelt[37] modeled image charge effects by an infinite series of ficticious charges placed along the z axis. A more comprehensive study by Brown *et al.*[38] includes cavity shifts in the cyclotron motions. Van Dyck *et al.*[39] modeled image charges by replacing the trap with a grounded conducting shell.

An approximate treatment of image charge effects proceeds in the following way.[35] The electric potential produced near the electrodes by a small plasma (i.e., $L/2, r_p \ll z_0$) of total charge Q in the center of the trap should be well approximated by the first terms in its multipole expansion, and dominated by the monopole term, which has the simple form $\Phi_m = Q/r$. The surface charge distribution drawn onto the electrodes to maintain their equipotentials must produce a potential $-Q/r$ at the electrode surface. If the electrodes formed a spherical shell, this would be accomplished by a charge distribution that itself had only a monopole term. For more complex electrodes, the potential produced inside the trap by the image charge may be expanded as

$$\Phi_I(r,\theta)=\frac{Q}{z_0}\sum_{l=0}^{\infty} B_l\left(\frac{r}{z_0}\right)^l P_l(\cos\theta),$$

where azimuthal symmetry has been assumed. The unitless coefficients B_l are determined by the requirement $\Phi_I(r(\theta),\theta)=-Q/r(\theta)$, where $r(\theta)$ is the equation of the electrode surfaces. Near the center of the trap, only the lowest-order terms are important. The monopole term ($l=0$) represents an unimportant shift in the zero of the potential. For electrodes that are symmetric about $z=0$, the coefficients vanish for odd values of l, so there is no dipole term. The quadrupole term ($l=2$) changes the trap quadrupole field from one described by the frequency ω_z to one described by ω_z^*, where

$$(\omega_z^*)^2=\omega_z^2-\frac{2qQ}{mz_0^3}B_2.$$

The spheroidal equilibrium and normal mode frequencies will be altered accordingly.

Downloaded 21 Jun 2001 to 132.239.73.116. Redistribution subject to AIP license or copyright, see http://ojps.aip.org/pop/popcr.jsp

For the special case of the center-of-mass mode, the assumption that odd-l coefficients vanish is not valid, because the plasma has a time-varying dipole moment. A treatment similar to that just described for the quadrupole image charge field induced by the monopole moment of the plasma may be used to calculate B_1 and higher coefficients. When the force on the plasma due to this time-dependent induced dipole is calculated, it is found to have the same effect on the center-of-mass motion as is produced by the static quadrupole field induced by the plasma monopole moment, resulting in harmonic oscillation at a frequency ω_{cm}, given by

$$\omega_{cm}^2=\omega_z^2-\frac{2qQ}{mz_0^3}(B_1+B_2). \tag{12}$$

Plasmas that are not much smaller than the trap may still have only minor effects from image charge, but the coefficients (possibly even their sign) will depend on the plasma length and radius, as well as the total charge. A numerical Poisson solution would be required to determine the image charge field for a particular plasma.

E. Anharmonicity

Deviations of the trap potential from a perfect quadrupole will affect the plasma equilibrium and the mode frequencies. The precision of a particular set of electrodes is customarily[40] described in terms of unitless coefficients in an expansion of the potential about the center of the trap:

$$\Phi(\rho,z)=V\frac{(z^2-\frac{1}{2}\rho^2)}{z_0^2}+V\sum_{l=0}^{\infty}C_l\left(\frac{r}{z_0}\right)^l P_l(\cos\theta). \tag{13}$$

In an ideal trap, all of the C_l coefficients are zero, and, in practice, all the odd-l coefficients are usually assumed to be negligible due to symmetry about $z=0$ maintained during the construction of the electrodes. The coefficient C_0 represents an unintentional (and unimportant) direct current (DC) offset to the potential, and C_2 describes a deviation of ω_z from its design value. The coefficient of the quartic term, C_4, is a measure of the trap imperfection, or anharmonicity. Precision traps have compensation electrodes in the asymptotic region of the trap, which make it possible to approximately zero C_4. The optimum configuration for this purpose is one that produces no change in C_2 as C_4 is adjusted, which is obtained for $\rho_0\simeq 1.16z_0$.[40] The asymptotically symmetric design approximated by our trap ($\rho_0=\sqrt{2}z_0$) is not the optimum, but has nevertheless been used for most precision trap experiments.

The coefficient, C_4, is a useful figure of merit for a trap, but does not sufficiently describe a trap if large plasmas are to be studied. A set of carefully chosen cylindrical electrodes can be made to null both C_4 and C_6 coefficients in the potential,[41] but will nonetheless deviate greatly from a quadrupole field near the electrodes, which do not lie along equipotentials of such a field. For large plasmas, or when large-amplitude motions of single trapped particles are expected, the hyperboloidal geometry shown in Fig. 1 may be preferable.

It is possible[35] to estimate the effect of a small trap anharmonicity on the mode frequencies. One of the most obvious effects of a substantial anharmonicity is that the plasma center-of-mass mode frequencies become dependent on the size and shape of the plasma.

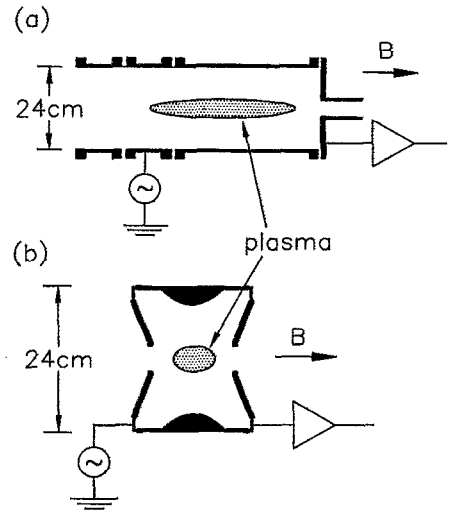

FIG. 3. Electrode assemblies showing the scheme for exciting and detecting plasma oscillations: (a) cylindrical trap; (b) approximate quadrupole trap.

III. DESCRIPTION OF THE EXPERIMENT

A. Plasma formation

The experimental device can produce single-component plasmas of positrons, electrons, or ions, which may be confined in a cylindrical electrode structure or in a set of hyperboloidal electrodes. Most of the data presented here are for electron plasmas. The positrons for the experiment were obtained from a ^{22}Na positron emitter used in conjunction with a thin-film tungsten moderator[42,43] or a solid neon moderator.[44,45] The tungsten moderator also provides a convenient source of electrons via secondary emission under positron bombardment. If the sign of all of the electrode potentials used for positron trapping is reversed, electrons can be trapped. The electron trapping rate can be adjusted to be comparable to the positron trapping rate. The confinement of electrons is very good, typically several hours, when the buffer gas is pumped out. This time scale appears to depend on the condition of the vacuum, and does not appear to follow the B^2/L^2 scaling law observed by Driscoll and Malmberg,[46] suggesting that the losses are dominated by a process other than conventional plasma transport processes. We suspect that the electron losses may involve attachment to neutral gas atoms or molecules, possibly water vapor. Because there are no annihilation losses, and the confinement time is high, the limit to the number of stored electrons appears to result from the plasma space charge, which can become comparable to the confinement potentials.

B. Hyperboloidal electrodes

Electron plasma experiments were performed with plasmas confined in both the cylindrical and the hyperboloidal electrode structures shown in Fig. 3. The unitless anharmo-

Downloaded 21 Jun 2001 to 132.239.73.116. Redistribution subject to AIP license or copyright, see http://ojps.aip.org/pop/popcr.jsp

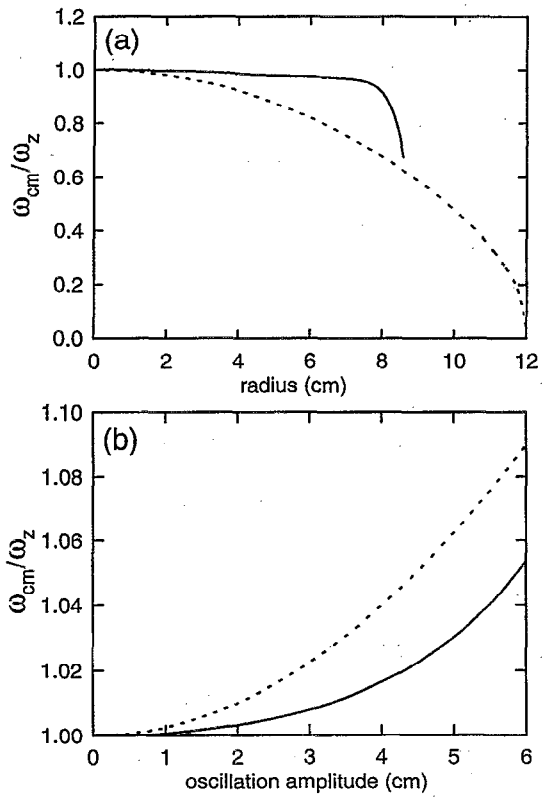

FIG. 4. Comparison of calculated anharmonicities of cylindrical electrodes (dotted curves) and approximate quadrupole electrodes (solid curves). (a) ω_{cm} vs ρ and (b): ω_{cm} versus the amplitude of oscillation.

nicity parameter for the cylindrical structure, defined by analogy to Eq. (13) but with the cylinder radius, r_w, replacing z_0 as the distance scale, is $C_4 \simeq 0.482$. Because of evidence, described in Sec. IV A, that the anharmonicity was affecting the plasma mode frequencies and impeding the remote detection of positrons, a new electrode structure, shown in Fig. 3(b), was designed to approximate the truncated hyperboloidal electrodes of a precision quadrupole trap. To reduce the effect on the differential pumping caused by obstruction, most of the surface of the endcaps consists of a mesh, with about 66% transmission. The 4.32 cm diam holes in the endcaps are required for positron filling. Numerical calculations with a Laplace solver indicated that with such large holes, there was no advantage in making the remainder of the endcaps precisely hyperboloidal, so a conical approximation to the hyperboloidal surface was made. The electrodes were made of aluminum and plated with gold on silver on copper.

The electrodes are designed to approximate an asymptotically symmetric quadrupole trap [see Eq. (1)] with $z_0 = 6.3$ cm. The anharmonicity coefficient for this structure is nominally $C_4 \simeq 0.055$, but is influenced by external potentials because of the large holes in the endcaps. Figure 4(a) shows the calculated axial bounce frequency as a function of radius for a single particle in the trap, showing a substantial improvement over the cylindrical structure. Another result of anharmonicity is the variation of the bounce frequency with bounce amplitude, shown in Fig. 4(b). A better comparison of the two traps is obtained if both values of C_4 are defined by the same distance scale. Using z_0 as the scale, the results are $C_4 \simeq 0.13$ for the cylindrical trap, compared to 0.055 for the quadrupole trap. The modest reduction in the anharmonicity resulted in large qualitative improvements in the data, as described below. In addition, the new electrodes are considerably closer to the plasmas, resulting in a great improvement in signal coupling to the plasmas.

C. Density measurement

The radial distribution of charge stored in the trap can be measured by reducing the voltage on one of the confining electrodes, causing the trapped particles to stream out of the confinement region along the magnetic field lines. The "dumped" charge strikes a set of 11 concentric annular collector plates. The collector array is located outside the main solenoid, so the diverging field lines give a view of the plasma magnified by $\sqrt{B_0/B_c} \simeq 1.76$, where B_c is the magnetic field at the collectors. This results in a radial spatial resolution at the plasma of 0.27 cm for the inner eight collectors. The collectors are gold-plated aluminum machined to overlap so that all charge within the outer radius of the array is collected, avoiding charging of the support block.

Dividing the charge measured on a collector by the area to which it maps gives a measure of the z-integrated plasma density, q_z, at the average radius to which the collector maps. To infer plasma density from these z-integrated profiles requires a numerical calculation, in which Poisson's equation, $\nabla^2\Phi(\rho,z) = -4\pi q n(\rho,z)$, is solved with the proper electrode geometry and potentials. It is assumed that the plasma is in local thermal equilibrium along each magnetic field line and that there is no azimuthal variation, so that the density at each radius has a Boltzmann distribution,

$$n(\rho,z) = q_z(\rho) C(\rho,T) e^{-q\Phi(\rho,z)/k_B T}, \tag{14}$$

where Φ is the total potential, including the self-consistent field of the plasma. Here $C(\rho,T)$ is a normalization constant associated with the Boltzmann factor, and $q_z(\rho)$ is the z integral of $n(\rho,z)$, the data input to the program. In principle, the plasma temperature, T, could be a function of ρ, as might occur if rapid radial transport leads to Joule heating, but we always assume a uniform temperature, which is usually 300 K. As described below, the temperature is confirmed by direct measurement to within an accuracy of 20% at 300 K. The computer program makes a guess of the total potential and distributes the known number of particles at each radius according to this potential using Eq. (14). It then solves Poisson's equation to find a new estimate for Φ, and iterates the procedure until adequate convergence is achieved.

D. Temperature measurement and heating

We use the standard "magnetic beach" technique to measure the temperature of the plasmas.[47,48] A small water-cooled coil is positioned behind the collector array and its current is adjusted to make the total magnetic field at the collectors equal to the field in the confinement region. A

Downloaded 21 Jun 2001 to 132.239.73.116. Redistribution subject to AIP license or copyright, see http://ojps.aip.org/pop/popcr.jsp

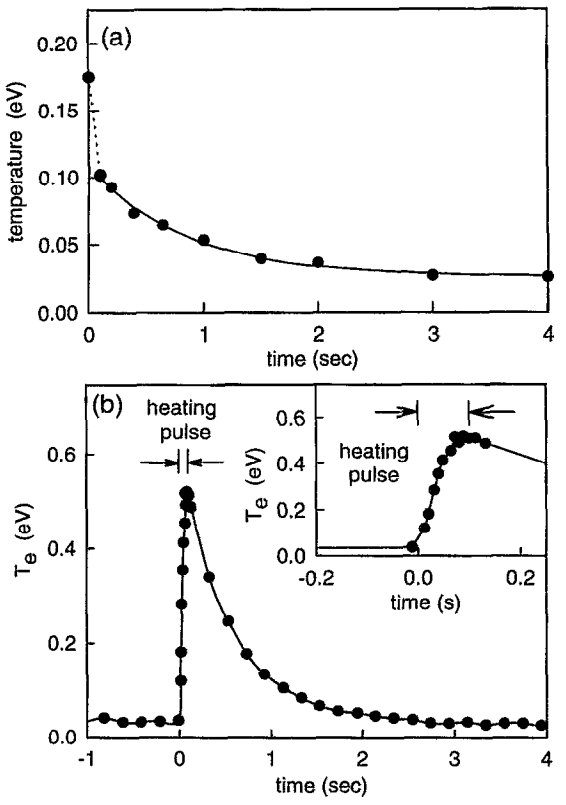

FIG. 5. (a) Temperature as a function of time after trapping. (b) Plasma heating by RF noise, followed by cooling on the buffer gas. The inset shows the temperature rise during heating pulse with a saturation at $k_B T \simeq 0.5$ eV.

series of nominally identical plasmas are formed and dumped with varying potential biases V_b on the collectors, and the total charge received is recorded. In principle, this curve contains information on the velocity distribution of the plasma and can be used to deduce the plasma temperature,[49] but this is complicated by the changes to the plasma potential that occur as the plasma is dumped. Instead, the field at the collectors is increased to produce a magnetic mirror, and the dataset is retaken. The slopes of the two curves at their midpoints are used to estimate $\partial N/\partial V_b$, and the separation between the curves gives an estimate of $\partial N/\partial R$, where R is the mirror ratio. The temperature is the ratio of these quantities,

$$k_B T = q \frac{\partial N/\partial R}{\partial N/\partial V_b}.$$

Temperature measurements made at varying times after the rapid introduction of a small number of particles into the trap allow the cooling of the particles by collisions with the buffer gas to be observed. As shown in Fig. 5(a), there is an initial rapid cooling immediately after the filling is shut off and thereafter, the plasma approaches its final temperature with an exponential cooling time constant, which is typically $\tau_c \simeq 0.6$ s and depends on the buffer gas pressure. We have assumed that this final temperature is the temperature of the buffer gas, i.e., 300 K, and used this to calibrate the measurement. The resulting scale factor of 0.85 probably arises from imperfections in the geometry of this magnetic beach, principally the variation in the strength of the mirror field over the surface of the collector array and the location of the collectors outside the main solenoid. This variation leads to an uncertainty in defining the mirror ratio, R.

The plasma may be heated to about 0.5 eV by the application of short pulses ($\Delta t \sim 2-50$ ms) of broadband radio frequency (RF) noise ($\Delta f \sim 10$ MHz) to one of the electrodes.[12] The plasma temperature rises quickly to a maximum, above which it appears that an inelastic collision process, such as vibrational excitation of N_2 molecules, provides strong enough cooling to stabilize the temperature. After the heating pulse is switched off, the plasma cools toward room temperature on a time scale of a few seconds. To study plasmas of a particular temperature in the range $0.025 \leq k_B T < 0.5$ eV, we wait for the appropriate time after the application of a standard heating pulse. A typical cycle of RF heating and buffers gas cooling is shown in Fig. 5(b). The cooling time scale is different from panel (a) of this figure because a different buffer gas pressure was used.

E. Mode excitation and detection

Normal modes of the plasma are studied by applying sinusoidal signals to one electrode and measuring the signals induced on another electrode. As shown in Fig. 3, the two end electrodes are used for the study of modes with no azimuthal variation. A spectrum analyzer with a tracking generator is used to excite resonances by sweeping the excitation frequency. Typical mode frequencies are a few megahertz for the axial modes of electron plasmas. When a large amplitude of the drive signal is used, heating effects can be seen in the form of a reduction of the signal amplitudes and shifts in frequency. The drive amplitudes were reduced to the point where these effects were no longer evident.

IV. EXPERIMENTAL RESULTS

Plasma experiments in the cylindrical electrode structure began with the simple goal of remote detection and monitoring of trapped positrons in the original three-stage positron trap. This turned out to be surprisingly difficult because of the small numbers of positrons then available (3×10^5), various signal-coupling problems, and an unexpected physical effect that was eventually ascribed to the anharmonic nature of the trap potential. In addition, the normal modes of large electron plasmas, though easily excited and detected, could not be accurately compared with theories for either cylindrical or spheroidal plasmas. This led to the design of the hyperboloidal electrode structure described in Sec. III B and to a substantial improvement in the data. Small numbers of particles (about 10^4 or more) could be detected by exciting and detecting an oscillation of their center of mass about the center of the trap. The electron plasma mode frequencies were found to be much more stable, but were still not in quantitative agreement with the cold fluid theory for spheroidal plasmas [Eq. (11) and Fig. 2]. The discrepancy was discovered to be mainly the result of the finite plasma temperature. This effect has been studied in detail for the lowest-order axial plasma mode, the quadrupole mode.

Downloaded 21 Jun 2001 to 132.239.73.116. Redistribution subject to AIP license or copyright, see http://ojps.aip.org/pop/popcr.jsp

A. Cylindrical trap

1. Electrostatics

As shown in Fig. 3(a), the electrodes of the third stage of the positron trap consist of three cylinders and a flat disk-shaped electrode with a hole in the center for particle access. The end cylinder is set to a potential V_1, the disk electrode is set to V_2, and the middle two cylinders are grounded. The plasmas studied are contained well within the long cylinder, so that the hole in the disk and the details of the geometry beyond the second short cylinder are not important. As a result, the basic features of the electrostatics of the trap can be determined analytically from the Green's function for a closed cylinder[50] by placing a fictitious disk at the far end of the second short cylinder. Useful results that can be obtained include the location of the potential minimum and the expansion of the potential about the minimum [as in Eq. (13)], as functions of the potentials on the disk electrode and the short cylinders with respect to the long cylinder. The results are in good agreement with more laborious numerical solutions to Laplace's equation.

A simpler approach that gives very similar results uses only the dominant terms of the expansion for the trap potential obtained from the Green's function. This gives the form

$$\Phi(\rho,z)\simeq J_0\left(\frac{x_{01}\rho}{r_w}\right)(V_1c_1e^{-x_{01}z/r_w}+V_2c_2e^{x_{01}z/r_w}), \quad (15)$$

where J_0 is a Bessel function, $x_{01}\simeq 2.4048$ is the first zero of $J_0(x)$, c_1 and c_2 are constants, and $z=0$ is defined as the geometrical center of the trap. The exponentials are approximations to hyperbolic sine functions. Considering the potential along the axis ($\rho=0$), we can easily find the position of the minimum,

$$z_c\simeq\frac{r_w}{2x_{01}}\ln\left(\frac{c_1V_1}{c_2V_2}\right), \quad (16)$$

and the power series expansion of $\Phi(0,z)$ about the minimum, which is recognized as a hyperbolic cosine function, giving the result

$$\Phi(\rho,z)\simeq 2(c_1c_2V_1V_2)^{1/2}J_0\left(\frac{x_{01}\rho}{r_w}\right)\cosh\left(\frac{x_{01}(z-z_c)}{r_w}\right). \quad (17)$$

The frequency of small oscillations about z_c is found to be

$$\omega_z(\rho)\simeq\left[J_0\left(\frac{x_{01}\rho}{r_w}\right)\right]^{1/2}\left(\frac{4q^2x_{01}^4}{m^2r_w^4}c_1c_2V_1V_2\right)^{1/4}. \quad (18)$$

Equation (17) is a generic form for the potential near a minimum inside a long cylinder. Different geometries of the end electrodes, different cylinder lengths, and different choices for the location of $z=0$ affect only the coefficients c_1 and c_2, as long as V_1 and V_2 are not so different that the potential minimum is close to one of the end electrodes. The insensitivity of z_c to V_1 and V_2 indicated by Eq. (16) is a problem if a center-of-mass oscillation is to be excited by oscillating V_1 and detected by signals induced on V_2. A more physical explanation is that external fields die out exponentially with distance inside a conducting cylinder, which is the essence of Eq. (15). The anharmonicity of the potential is easily found from the power series for the hyperbolic cosine. A distance scale must be chosen [for example, in Eq. (13), coordinates are scaled by z_0], and the natural choice in this geometry is the radius of the cylinder wall, r_w. This results in $C_4=x_{01}^2/12$, i.e., $C_4\simeq 0.482$, for any long cylindrical trap. The positive sign of C_4 indicates that the potential well "stiffens" with increasing distance from the minimum.

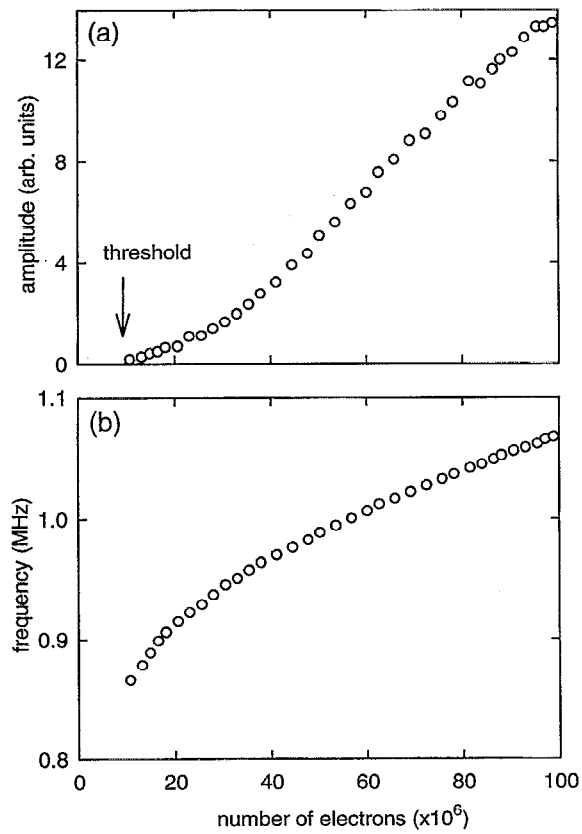

FIG. 6. Dependence of (a) amplitude and (b) frequency of the axial center-of-mass oscillation on the number of particles in the cylindrical trap.

2. Center-of-mass mode

For clouds of particles in which space charge effects are negligible, the particles will collect about the axial potential minimum, with the radial distribution with which they are trapped. If their radial distribution is narrow and their temperature is low enough that they stay close to the minimum, the potential is approximately quadrupole, leading to small-amplitude harmonic oscillations at the frequency, $\omega_z(0)$, given in Eq. (18). A coherent excitation of all the particles produced by a sinusoidal signal applied to one of the short cylinders will result in the oscillation of their center of mass at the frequency $\omega_{cm}=\omega_z(0)$, which will produce a signal proportional to N on the disk electrode.

This simple result was never observed with the cylindrical electrodes. Instead, it was found that unexpectedly large numbers of particles were required to produce a detectable signal ($N\sim 10^7$), that this signal occurred at a frequency $\omega_{cm}>\omega_z(0)$, and that the amplitude of the signal was a nonlinear function of N and of other uncontrolled variables. Fig-

Downloaded 21 Jun 2001 to 132.239.73.116. Redistribution subject to AIP license or copyright, see http://ojps.aip.org/pop/popcr.jsp

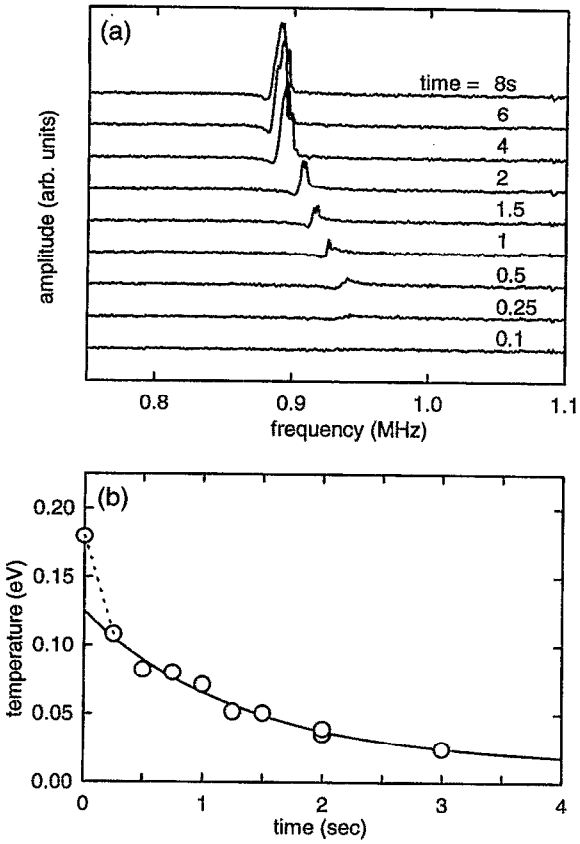

FIG. 7. (a) Center-of-mass response spectra, for about 10^7 electrons in the cylindrical trap, at varying times after a rapid fill. The curves are offset vertically for clarity. (b) Cooling curve measured under the same conditions.

ure 6 shows a typical dataset. Such large collections of particles are plasmas and elongate considerably due to their space charge, so it is reasonable that the signal coupling will improve and that the frequency may rise as the longer plasmas feel the trap anharmonicity more strongly.

What is surprising is that there is a threshold behavior to the response, such that the response detected for ($N \sim 10^7$) is relatively strong, but a 20% reduction in N below this results in a very small signal. A more telling result is that this threshold is correlated with temperature, as demonstrated in Fig. 7, where the response spectrum of 10^7 electrons is monitored as the plasma cools after a rapid fill. The response as a function of temperature for this dataset is shown in Fig. 8, which also shows the results for a plasma with half as many particles.

Because such an effect cannot easily be explained in a pure quadrupole potential, the trap anharmonicity appears to be a contributing factor. The dependences on T and N (which implies a dependence on n) could both be explained by the existence of a threshold value when the size of the plasma is comparable to the Debye length. It may be that the typical radial particle distribution, which is approximately Gaussian with a rms radius of about 1 cm, is wide enough to cause substantial phase mixing of the signals from particles at different radii because of the radial variation in ω_z indicated in Eq. (18) and in Fig. 4(a). Even particles at the same radius

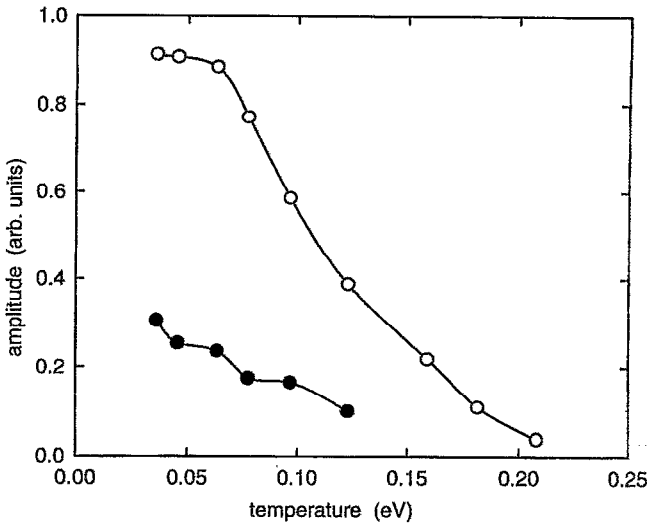

FIG. 8. Amplitude of center-of-mass response versus temperature: (○) data in Fig. 7; (●) half as many particles.

will have a distribution of bounce periods due to anharmonicity and the thermal distribution of amplitudes of oscillation, as shown in Fig. 4(b). A charge cloud with sufficient plasma character (i.e., one with $\lambda_D < \lambda_{threshold}$) would tend to move collectively and might avoid these damping mechanisms. It is not clear, at present, whether this phenomenon is related to the synchronization of particle motion observed in cryogenic traps with smaller numbers of particles.[51,52]

3. Plasmas

In spite of the difficulty of detecting small numbers of particles in the cylindrical trap, there is no trouble exciting and detecting various normal modes of large plasmas. A typical response spectrum, shown in Fig. 9, presents a family of resonances of increasing frequency excited by a sinusoidal signal applied to one of the confining electrodes (see Fig. 3). Density profiles of the plasmas, obtained by applying the Poisson solution program to charge collector data (as described in Sec. III C), appear roughly spheroidal, so an at-

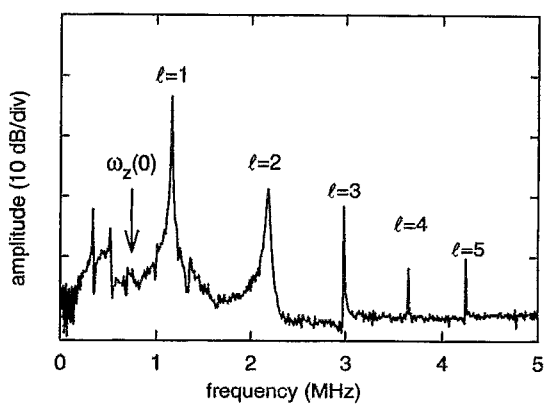

FIG. 9. Spectrum of a plasma of about 2×10^8 electrons in the cylindrical trap. Values of l refer to the mode theory for spheroids [Eq. (11)].

Downloaded 21 Jun 2001 to 132.239.73.116. Redistribution subject to AIP license or copyright, see http://ojps.aip.org/pop/popcr.jsp

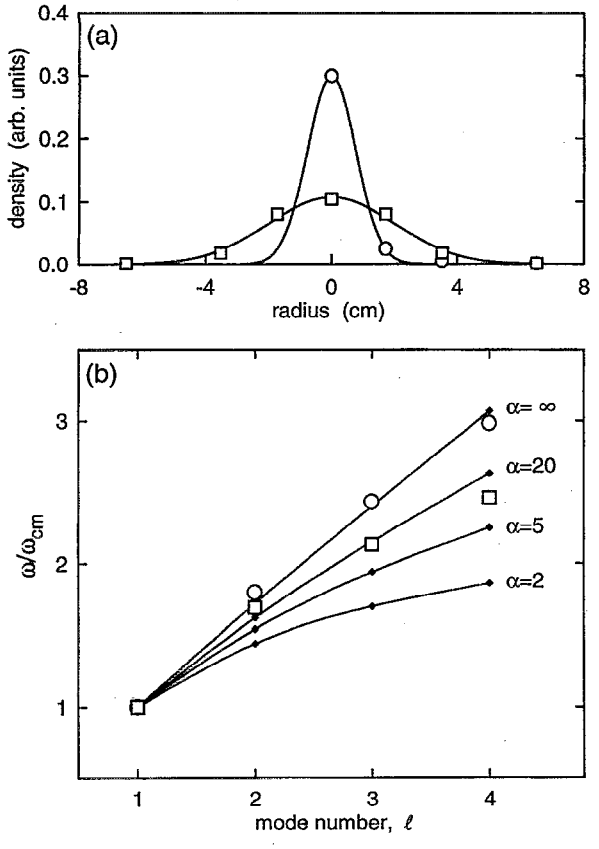

FIG. 10. (a) The z-integrated radial profiles for two plasmas in the cylindrical trap with similar numbers of particles and different aspect ratios: (○) $\alpha\sim 20$; (□) $\alpha\sim 5$. (b) Comparison of the frequencies of four modes in the plasmas shown in (a) with spheroidal mode theory shown by small points connected by smooth curves.

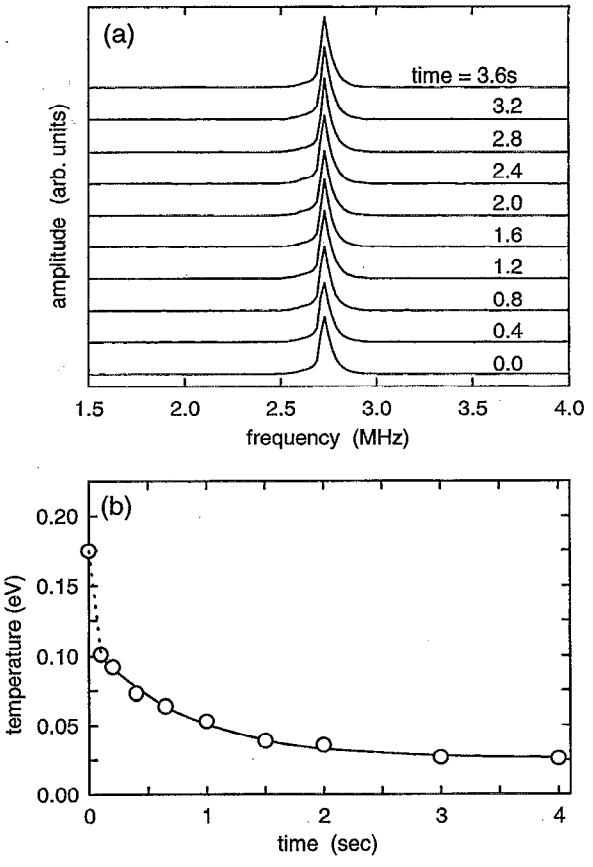

FIG. 11. (a) Center-of-mass response spectra of about 10^7 electrons in the quadrupole trap at varying times after a rapid fill. The curves are offset vertically for clarity. (b) Cooling curve measured under the same conditions.

tempt was made to analyze the data using the spheroidal mode theory [Eq. (11) and Fig. 2]. A strong response was expected at the value of $\omega_z(0)$ predicted by Eq. (18). As mentioned in the preceding section, the strongest response consistently occurred at a substantially higher frequency, but by decreasing N it was possible to track the mode frequency close enough to $\omega_z(0)$ to be confident of its identification as the center-of-mass oscillation. The higher-frequency series of modes were thus suspected to be the $l=2,3,4,\ldots$, axial modes predicted by the theory.

To test the dependence of the mode frequencies on aspect ratio, two similar plasmas with different aspect ratios were obtained by filling them under identical conditions and then reducing B in one case to expand the plasma radially, giving the z-integrated radial profiles shown in Fig. 10(a). The frequencies of the most prominent modes observed in each case are plotted in Fig. 10(b). The value of ω_{cm} was different for the two plasmas and was not close to $\omega_z(0)$ in either case, so the mode theory will clearly not be satisfied to any degree of precision. It was found that by scaling the frequencies by the measured values of ω_{cm} rather than $\omega_z(0)$, better agreement with the theory was obtained. Sets of frequencies predicted by the theory for four different aspect ratios are also shown in Fig. 10(a), connected by lines to distinguish them from the data points. These data show sufficient qualitative agreement with the behavior predicted by the cold fluid theory to be confident with the identification of the modes. For the radial profiles shown in Fig. 10(a) a low-resolution collector plate assembly consisting of only five rings was used. For this part of the experiment, this low resolution was not a great restriction because of the qualitative nature of the result. However, for the experiments described in Sec. IV B, where a quantitative analysis was made, the resolution of the collector plate assembly was improved by increasing the number of rings to 11.[11]

Two weaker modes are visible at frequencies less than $\omega_z(0)$ in the spectrum. Possible candidates for these modes are the $l=3$ and $l=4$ modes with radial structure indicated in Fig. 2.

B. Quadrupole trap

1. Center-of-mass mode

In the quadrupole trap, the nonlinear behavior of the axial center-of-mass mode seen in the cylindrical trap is absent. When data such as that shown in Fig. 7 is obtained in the quadrupole trap, the amplitude and frequency of oscillation appear to be independent of the plasma temperature, as shown in Fig. 11, in strong contrast to the trend shown in Fig. 7. Because of the increased sensitivity, it is possible to

Downloaded 21 Jun 2001 to 132.239.73.116. Redistribution subject to AIP license or copyright, see http://ojps.aip.org/pop/popcr.jsp

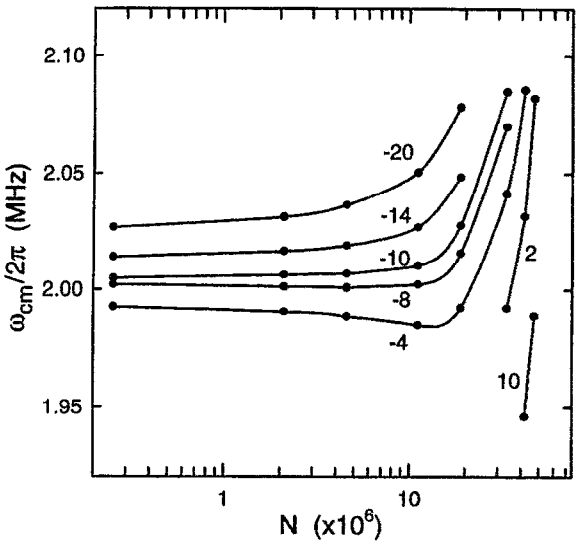

FIG. 12. Dependence of center-of-mass frequency on the number of particles, N, in the quadrupole trap for $V_{ring}=3.2$ V, $V_{endcaps}=0$ V. The numbers labeling the curves are the various external potentials.

track the amplitude of the response across the range of N over which the transition to a plasma should occur.

The dependence of ω_{cm} on N can be adjusted to some extent by varying the quadrupole trap potentials relative to the rest of the trap. This is shown in Fig. 12, in which curves of $\omega_{cm}(N)$ are taken for various values of the external potentials. The most obvious features are that it is possible to tune the anharmonicity to make ω_{cm} independent of N for $N<10^7$, but that for much higher n, ω_{cm} rises regardless of the anharmonicity.

The remainder of the data in this section were taken with the anharmonicity adjusted to minimize the variation of ω_{cm} with N, even though this did not occur at the expected values of the external potentials. It appears that, rather than nulling C_4, this procedure adjusted it to balance the initial effect of the increasing image charge.

2. Plasmas

Axial plasma modes are easily excited and detected in the quadrupole trap. A typical spectrum has strong $l=1$ and $l=2$ peaks, and sometimes either a weak $l=3$ peak or one or two weak low-frequency modes. For plasmas with small aspect ratios, the modes with frequencies less than ω_z can become prominent. Typical spectra taken in the quadrupole trap have significant qualitative differences from the spectra (such as Fig. 9) obtained in the cylindrical trap. The signal-to-noise ratio is greatly improved by the superior signal coupling, but fewer of the purely axial modes are detected, probably because of the different plasma shapes studied in the two traps. The geometry of the hyperboloidal trap enforces the restriction $L<2z_0$ on the plasma length. Because of the condition $\lambda_D \ll \lambda$ for undamped plasma modes, discussed in Sec. II C, fewer axial modes are expected for a short plasma. This is the only disadvantage that we have found to using the quadrupole trap.

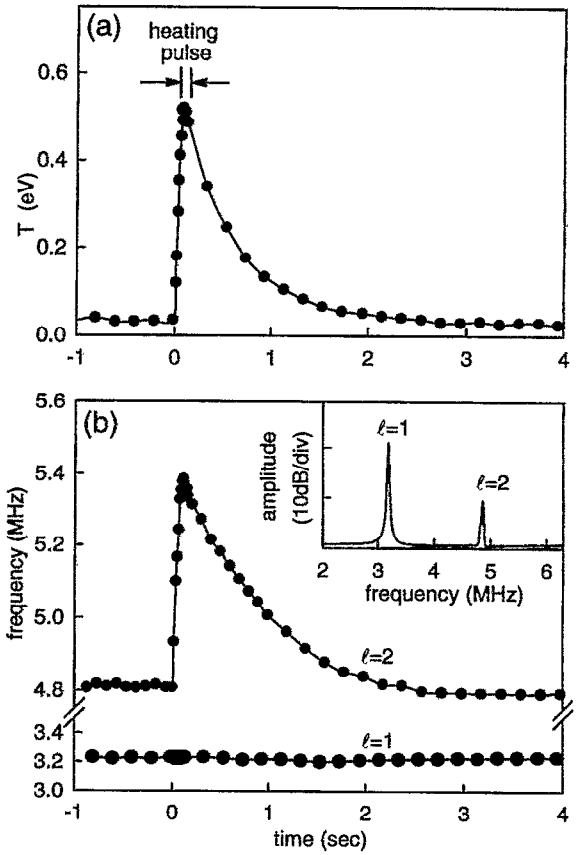

FIG. 13. (a) Temperature during a cycle of RF heating and cooling on the buffer gas. (b) Frequencies of the center-of-mass ($l=1$) and quadrupole ($l=2$) modes during the heating cycle shown in (a). A spectrum for $t<0$ is shown in the inset.

3. Temperature dependence of quadrupole mode

The technique described previously of reducing the magnetic field B to obtain similar plasmas with different aspect ratios was used to measure the dependence of the quadrupole ($l=2$) mode frequency on α, and a significant discrepancy with the cold fluid theory remained. Much of this difference is caused by the nonzero temperature of the plasma. Figure 13(b) plots the frequency of the quadrupole mode measured at various times during a cycle of RF heating and cooling, with the plasma temperature shown in Fig. 13(a). This figure also shows the frequency of the center-of-mass mode, and as expected, no significant temperature dependence is observed. Figure 14(b) shows the quadrupole mode frequency as a function of temperature for three plasmas with different aspect ratios. The radial profiles are shown in Fig. 14(a). When the data are extrapolated to $T=0$, frequencies within about 1% of the cold fluid predictions for the quadrupole mode are obtained, confirming our identification of the mode.

The cold fluid theory assumes a cold plasma of uniform density in an exactly quadratic potential imposed by distant electrodes. To model effects not included in the cold fluid theory, Spencer and Mason performed numerical simulations of the plasmas.[10] The electrode voltages and z-integrated density profiles of experimentally measured plasmas were

Downloaded 21 Jun 2001 to 132.239.73.116. Redistribution subject to AIP license or copyright, see http://ojps.aip.org/pop/popcr.jsp

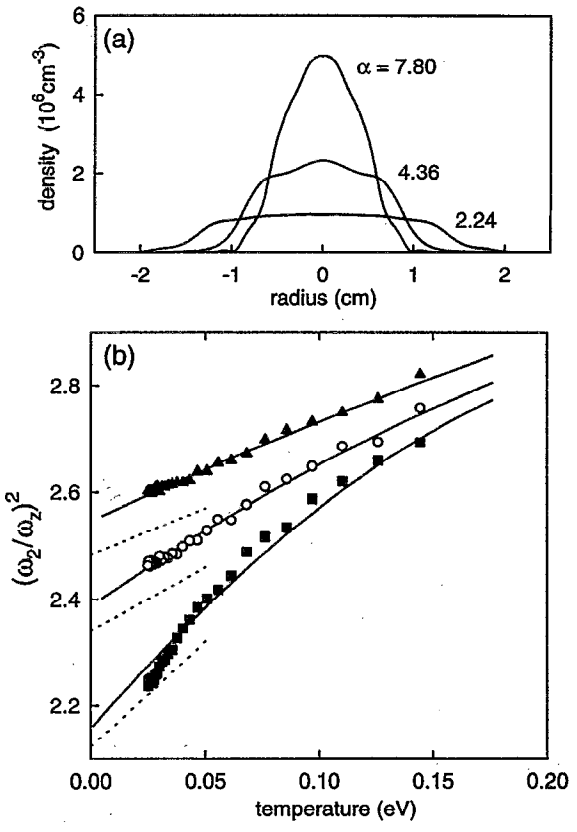

FIG. 14. (a) Radial density profiles in the plasma midplane for three electron plasmas with similar numbers of particles but different aspect ratios. (b) Temperature dependence of the quadrupole mode frequency for the plasmas shown in (a): (□) α=2.24, L=6.20 cm; (○) α=4.38, L=7.52 cm; (△) α=7.80, L=8.32 cm. The solid lines are numerical simulations and the dotted lines are from the fluid theory using Eq. (19).

used as input to a Poisson–Boltzmann equilibrium code. The resulting equilibria, from which the plasma aspect ratios were obtained, were constrained to match the experimental density profiles and the total particle number. The computations were done assuming axisymmetry and used a 120 by 240 grid for the coordinates ρ and z.

The computed equilibria were then used to create initial distributions for particle-in-cell simulations that used the same spatial grid and electrode representation as the equilibrium computation. The center-of-mass and quadrupole modes were excited by displacing all of the particles by a small amount in the same direction in z and also by stretching the plasma along the z axis. The position of the center of mass, z_{cm}, and the density average of the square of the position of the plasma relative to the center of mass $\langle(z-z_{cm})^2\rangle$, were then tracked in time and Fourier analyzed to yield the frequencies of the center-of-mass and quadrupole modes, respectively. The plasma was represented by 50 000 particles, which were advanced through 16 384 time steps of 4×10^{-9} s each.

The experimentally measured plasmas shown in Fig. 14 were studied using these simulation techniques. From the Poisson–Boltzmann code, the aspect ratios were found to be 7.80, 4.38, and 2.24. For each aspect ratio, simulations were made for ten temperatures in the range 0.001–0.176 eV. The predicted frequency ratio between the quadrupole and center-of-mass modes shown by the solid lines in Fig. 14 is in excellent agreement with the data. The simulation frequencies at the lowest temperatures agree well with the predictions of Dubin's cold fluid theory (i.e., to within 3%), as shown in Fig. 14(b). This is interesting in view of the fact that the density profiles shown in Fig. 14(a) differ substantially from the nearly uniform density expected for a plasma in global thermal equilibrium (and assumed by the cold fluid theory). The insensitivity of the mode frequencies to the plasma profile simplifies their use as diagnostics, as discussed in Sec. IV C.

An approximate analytical treatment of temperature effects on the quadrupole mode frequency was proposed recently by Dubin.[33] This model leads to a prediction of a shift in the quadrupole mode frequency from the cold fluid result ω_2^c to ω_2:[35]

$$(\omega_2)^2=(\omega_2^c)^2+20[\gamma-g(\alpha)]\frac{k_BT}{mL^2}, \tag{19}$$

with

$$g(\alpha)=\frac{\alpha^2}{2}\frac{\omega_p^2}{(\omega_2^c)^2}\frac{\partial^2A_3}{\partial\alpha^2}, \tag{20}$$

where $A_3(\alpha)$ is defined in Eq. (7) and γ=3 is the ratio of specific heats for one-dimensional expansions. All quantities on the right-hand sides of Eqs. (19) and (20) are evaluated in the cold fluid limit. The function $g(\alpha)$ describes the frequency shift from the temperature dependence of the plasma shape. If this term is neglected, one obtains a result similar to the Bohm–Gross dispersion relation for a warm neutral plasma, $\omega^2=\omega_p^2+\gamma k_z^2k_BT/m$, with $k_z\simeq\pi(l-1)/L$.

The data shown in Fig. 14 indicate that $(\omega_2)^2$ is linear in T for the longer plasmas, but deviates from linearity for the shortest plasma, for which the temperature dependence is strongest. For the same value of T and the same mode, the effect of temperature is stronger for shorter plasmas because the wavelength of the mode is smaller, making the effective temperature higher. The slopes of the curves at low temperatures agree reasonably well with the predictions of Eq. (19), which are plotted as dashed lines in Fig. 14.

C. Diagnostic applications

For positron and positron–electron plasmas, nondestructive diagnostics are essential, and the measurement of the frequencies of plasma modes is an attractive way of accomplishing this, because frequencies can be measured with great precision. The modes studied are global, and thus they provide information on global plasma parameters. For the purposes of mode studies, the spatial distribution is adequately parametrized by L and α, since the mode frequencies are relatively insensitive to the radial density profile. Therefore, the cold fluid equilibrium theory for a uniform-density spheroid [Eq. (6)] may be used to relate the parameters N, α, and L:

$$L^3=\frac{12e^2}{m\omega_z^2}\alpha^2A_3(\alpha)N. \tag{21}$$

Downloaded 21 Jun 2001 to 132.239.73.116. Redistribution subject to AIP license or copyright, see http://ojps.aip.org/pop/popcr.jsp

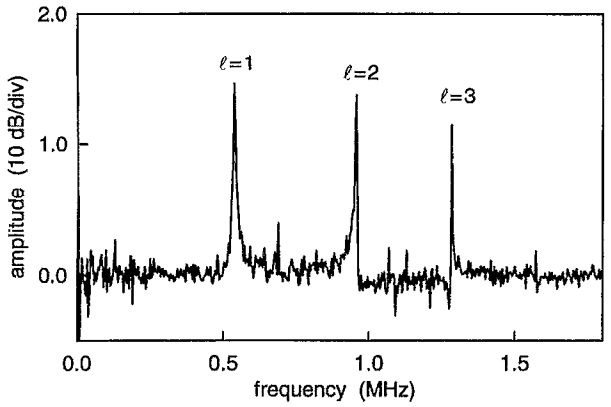

FIG. 15. Spectrum of a positron plasma of 6×10^7 particles in the cylindrical trap.

Thus, a measurement of N fixes a relationship between L and α. Measurement of two plasma modes combined with the results of simulations or warm fluid theory would provide the additional relationships to uniquely determine L, α, and T, and hence also the plasma radius and density. If the temperature is known, as it is in the presence of a buffer gas, then with N determined from the amplitude of the center-of-mass response, Eqs. (19) and (21) may be used to determine L and α from the quadrupole mode frequency. Once the plasma parameters are established, whether by these techniques or by other diagnostics, subsequent changes in either temperature or shape may be deduced from additional shifts in a single-mode frequency, as in the data for ω_2 during a heating pulse, shown in Fig. 13. Alternatively, if the temperature can be controlled, the plasma length and aspect ratio may be found from the slope and intercept of data for $(\omega_2)^2$ vs T. Applying this technique to the data in Fig. 14, we obtain lengths of 8.5, 7.3, and 5.3 cm for the three plasmas, while the experimental values are 8.3, 7.5, and 6.2 cm, respectively.

The use of data from modes other than the quadrupole mode would benefit greatly from a complete theory of finite-temperature spheroidal plasmas. Modes with azimuthal structure, such as the $l=2$, $m=2$ diocotron modes, have frequencies that depend on aspect ratio,[7] and they could provide the data needed for complete determination of the bulk plasma parameters, if their temperature dependence were understood.

D. Positron plasmas

All the preceding data were obtained using electrons. At the time of the early work in the cylindrical trap, the largest positron plasmas consisted of about 10^6 positrons, and due to the anomalous damping and the poor sensitivity of the cylindrical trap, even their center-of-mass motion could not be detected. With the construction of the quadrupole trap, the sensitivity improved and the anomalous damping was eliminated, permitting the detection of the center-of-mass motion of as few as 10^4 positrons, but no plasma modes were seen.

With the replacement of the tungsten-film positron moderator by a more efficient solid neon moderator, plasmas containing more than 10^8 positrons can now be obtained. Figure 15 is a mode spectrum obtained for such a positron plasma confined in the cylindrical trap, where the positron trapping efficiency is highest. Strong signals are seen for the center-of-mass oscillation and for the $l=2$ and $l=3$ axial plasma modes. This is the first time that collective modes of an antimatter plasma have been observed. As with the electron plasmas, fewer modes are observed in the quadrupole trap, but the quadrupole mode is seen.

V. CONCLUSIONS

We have studied the normal modes of single-component plasmas in cylindrical and hyperboloidal geometry, and for the latter case, we have found good agreement with the comprehensive normal mode theory of Dubin. This study complements the work on cold ion microplasmas,[8,9] in which excellent agreement with the theory has been obtained for the frequencies of the quadrupole mode and the $l=2$, $m=1$ modes. Under the proper conditions, confidence in the theory is sufficient to justify its use as a measurement tool, as in the studies by Weimer[53] of cryogenic electron plasmas.

Because some of the conditions of our experiments are set by considerations other than the production of small, cold, precisely spheroidal plasmas, we have considered the effects of various perturbations. Important effects of which we are aware include those due to image charges, nonuniform density profile, trap anharmonicity, and plasma temperature. At this point, some progress has been made in understanding the frequency shifts caused by finite temperature, which can now be used to measure this important parameter. By varying N, varying the trap anharmonicity, and allowing electron plasmas time to reach equilibrium after pumping out the buffer gas, it may be possible to unravel the separate effects of the remaining perturbations, and such experiments are planned. The success of the numerical simulations by Spencer and Mason in matching the quadrupole mode data suggests that such calculations could be of great use in studies of this type. That all these complications may be treated as small perturbations to the cold fluid theory suggests that the theory will continue to be of great utility.

Quadrupole traps and spheroidal plasmas offer the opportunity to approach some of the unsolved problems of nonneutral plasmas from a new perspective. If a phenomenon in question has been tentatively identified as a "three-dimensional" (3-D) effect in cylindrical plasmas, it might be interesting to repeat the experiment with spheroidal plasmas, in which the 3-D nature is under experimental control, and is perhaps better understood. The features that make quadrupole traps appealing to atomic physicists, the exactly soluble simple harmonic motions of single particles and their long confinement time, may make studies of plasmas in quadrupole traps an interesting test of field-error-driven transport, since resonances with field errors could be very strong (the harmonic frequencies do not shift off resonance as the amplitude of motion grows) and would be shared by all particles, if space charge is negligible. Because good confinement does not require the strong self-field of a well-developed plasma, it may also be possible to learn about the nature of marginal plasmas and of the transition from inde-

Downloaded 21 Jun 2001 to 132.239.73.116. Redistribution subject to AIP license or copyright, see http://ojps.aip.org/pop/popcr.jsp

pendent particle motions to the collective behavior of a plasma.

ACKNOWLEDGMENTS

We are indebted to D. H. E. Dubin for many valuable suggestions and discussions regarding this work. We gratefully acknowledge discussions with T. M. O'Neil, C. F. Driscoll, and K. S. Fine. We are pleased to acknowledge the fruitful collaboration that has developed with R. L. Spencer and G. W. Mason.

This work was supported by the Office of Naval Research.

APPENDIX: ANALYTICAL FORMULAS FOR SPHEROIDAL PLASMAS

An explicit form for the spheroidal equilibrium, expressed in terms of Q_1^0 in Eq. (6), is

$$\frac{\omega_p^2}{\omega_z^2}=\begin{cases}(1-\alpha^2)^{3/2}(\sqrt{1-\alpha^2}-\alpha\arcsin\sqrt{1-\alpha^2})^{-1}, & \text{for } \alpha<1,\\ (\alpha^2-1)^{3/2}\{(\alpha/2)\ln[(\alpha+\sqrt{\alpha^2-1})/(\alpha-\sqrt{\alpha^2-1})]-\sqrt{\alpha^2-1}\}^{-1}, & \text{for } \alpha>1.\end{cases} \tag{A1}$$

This corresponds to $1/B(\alpha)$, in the notation of Ref. 8.

The frequency of the quadrupole mode of a cold, strongly magnetized spheroidal plasma has the form

$$\left(\frac{\omega_2^c}{\omega_z}\right)^2=1+\frac{\alpha^2}{\alpha^2-1}\frac{(\alpha^2+\frac{1}{2})\ln[(\alpha+\sqrt{\alpha^2-1})/(\alpha-\sqrt{\alpha^2-1})]-3\alpha\sqrt{\alpha^2-1}}{(\alpha^2/2)\ln[(\alpha+\sqrt{\alpha^2-1})/(\alpha-\sqrt{\alpha^2-1})]-\alpha\sqrt{\alpha^2-1}}, \tag{A2}$$

for $\alpha>1$, the case typical of our electron plasmas.

Finally, a few notes on the roots of the dispersion relation of axial modes for the strongly magnetized case. The dispersion relation, Eq. (11), may be written in the form

$$(k_1^2-1)P_l'(k_1)=w_l(\alpha)k_1P_l(k_1), \tag{A3}$$

where $k_1=\alpha(\alpha^2-1+\omega_p^2/\omega^2)^{-1/2}$ and

$$w_l(\alpha)=\frac{1}{\alpha\sqrt{\alpha^2-1}}\frac{Q_l^{0\prime}(\alpha/\sqrt{\alpha^2-1})}{Q_l^0(\alpha/\sqrt{\alpha^2-1})}. \tag{A4}$$

Equation (A3) is a polynomial in k_1 of order $l+1$, with coefficients that depend on α. For even values of l, a factor of k_1 divides out. For any l, the result is a polynomial in k_1^2 of order $[(l+1)/2]$, where "[ ]" denotes the maximum integer. Thus, there is one root for $l=1$ or $l=2$, and there are two roots for $l=3$ or $l=4$, etc. Each solution for k_1^2 at a particular value of α translates into the value of ω for the normal mode, scaled by ω_p. The different eigenvalues of ω obtained for the same values of l and m correspond to normal modes with different radial structure. The modes with purely axial structure have the highest frequencies.

[1]C. W. Roberson and C. F. Driscoll (editors), *Non-Neutral Plasma Physics*, AIP Conf. Proc. No. 175 (American Institute of Physics, New York, 1988).
[2]R. C. Davidson, *Physics of Non-Neutral Plasmas*, (Addison–Wesley, Redwood City, CA, 1990).
[3]J. H. Malmberg and J. S. de Grassie, Phys. Rev. Lett. **35**, 577 (1975).
[4]J. J. Bollinger, D. J. Wineland, and D. H. E. Dubin, Phys. Plasmas **1**, 1403 (1994).
[5]S. L. Gilbert, J. J. Bollinger, and D. J. Wineland, Phys. Rev. Lett. **60**, 2022 (1988).
[6]L. Turner, Phys. Fluids **30**, 3196 (1987).
[7]D. H. E. Dubin, Phys. Rev. Lett. **66**, 2076 (1991).
[8]D. J. Heinzen, J. J. Bollinger, F. L. Moore, W. M. Itano, and D. J. Wineland, Phys. Rev. Lett. **66**, 2080 (1991).
[9]J. J. Bollinger, D. J. Heinzen, F. L. Moore, W. M. Itano, D. J. Wineland, and D. H. E. Dubin, Phys. Rev. A **48**, 525 (1993).
[10]M. D. Tinkle, R. G. Greaves, C. M. Surko, R. L. Spencer, and G. W. Mason, Phys. Rev. Lett. **72**, 352 (1994).
[11]M. D. Tinkle, "Electrostatic oscillations of spheroidal single-component plasmas," Ph.D. thesis, University of California, San Diego, 1994.
[12]R. G. Greaves, M. D. Tinkle, and C. M. Surko, Phys. Plasmas **1**, 1439 (1994).
[13]R. G. Greaves, M. D. Tinkle, and C. M. Surko, Phys. Rev. Lett. **74**, 90 (1995).
[14]C. M. Surko, M. Leventhal, and A. Passner, Phys. Rev. Lett. **62**, 901 (1989).
[15]T. J. Murphy and C. M. Surko, Phys. Rev. A **46**, 5696 (1992).
[16]V. Tsytovich and C. B. Wharton, Comm. Plasma Phys. Controlled Fusion **4**, 91 (1978).
[17]N. Iwamoto, Phys. Rev. E **47**, 604 (1993).
[18]G. P. Zank and R. G. Greaves, Phys. Rev. E **51**, 6079 (1995).
[19]A. Mohri, H. Tanaka, T. Michishita, Y. Yuyama, Y. Kawase, and T. Takami, in *Elementary Processes in Dense Plasmas*, edited by S. Ichimara and S. Ogala (Addison–Wesley, Reading, MA, 1995), pp. 477–486.
[20]T. E. Cowan, B. R. Beck, J. H. Hartley, R. H. Howell, R. R. Rohatgi, J. Fajans, and R. Gopalan, Hyperfine Interact. **76**, 135 (1993).
[21]C. M. Surko, M. Leventhal, W. S. Crane, A. Passner, and F. Wysocki, Rev. Sci. Instrum. **57**, 1862 (1986).
[22]T. E. Cowan, J. Hartley, R. H. Howell, J. L. McDonald, R. R. Rohatgi, and J. Fajans, Mat. Sci. Forum **105–110**, 529 (1992).
[23]C. M. Surko, A. Passner, M. Leventhal, and F. J. Wysocki, Phys. Rev. Lett. **61**, 1831 (1988).
[24]T. J. Murphy and C. M. Surko, Phys. Rev. Lett. **67**, 2954 (1991).
[25]S. Tang, M. D. Tinkle, R. G. Greaves, and C. M. Surko, Phys. Rev. Lett. **68**, 3793 (1992).
[26]C. M. Surko, R. G. Greaves, and M. Leventhal, Hyperfine Interact. **81**, 239 (1993).
[27]K. Iwata, R. G. Greaves, T. J. Murphy, M. D. Tinkle, and C. M. Surko, Phys. Rev. A **51**, 473 (1995).
[28]D. J. Wineland, C. S. Weimer, and J. J. Bollinger, Hyperfine Interact. **76**, 115 (1993).
[29]M. Charlton, J. Eades, D. Horvath, R. J. Hughes, and C. Zimmermann, Phys. Rep. **241**, 65 (1994).
[30]G. Gabrielse, X. Fei, L. A. Orozco, R. L. Tjoelker, J. Haas, H. Kalinowsky, T. A. Trainor, and W. Kells, Phys. Rev. Lett. **63**, 1360 (1989).
[31]M. H. Holzscheiter, Hyperfine Interact. **81**, 71 (1993).
[32]T. M. O'Neil and C. F. Driscoll, Phys. Fluids **22**, 266 (1979).
[33]D. H. E. Dubin, Phys. Fluids B **5**, 295 (1993).
[34]A. W. Trivelpiece and R. W. Gould, J. Appl. Phys. **30**, 1784 (1959).
[35]D. H. E. Dubin (personal communication, 1994).
[36]R. L. Spencer (personal communication, 1994).
[37]D. J. Wineland and H. G. Dehmelt, J. Appl. Phys. **46**, 919 (1975).
[38]L. S. Brown, K. Helmerson, and J. Tan, Phys. Rev. A **34**, 2638 (1986).

Downloaded 21 Jun 2001 to 132.239.73.116. Redistribution subject to AIP license or copyright, see http://ojps.aip.org/pop/popcr.jsp

[39]R. S. Van Dyck, Jr., F. L. Moore, D. L. Farnham, and P. B. Schwinberg, Phys. Rev. A **40**, 6308 (1989).
[40]L. S. Brown and G. Gabrielse, Rev. Mod. Phys. **58**, 233 (1986).
[41]G. Gabrielse, L. Haarsma, and S. L. Rolston, Int. J. Mass Spectrometry Ion Proc. **88**, 319 (1989).
[42]E. Gramsch, J. Throwe, and K. G. Lynn, Appl. Phys. Lett. **51**, 1862 (1987).
[43]N. Zafar, J. Chevallier, F. M. Jacobsen, M. Charlton, and G. Laricchia, Appl. Phys. A **47**, 409 (1988).
[44]A. P. Mills, Jr. and E. M. Gullikson, Appl. Phys. Lett. **49**, 1121 (1986).
[45]R. Khatri, M. Charlton, P. Sferlazzo, K. G. Lynn, A. P. Mills, Jr., and L. O. Roellig, Appl. Phys. Lett. **57**, 2374 (1990).
[46]C. F. Driscoll and J. H. Malmberg, Phys. Rev. Lett. **50**, 167 (1983).
[47]D. Boyd, W. Carr, R. Jones, and M. Seidl, Phys. Lett. A **45**, 421 (1973).
[48]T. Hsu and J. L. Hirshfield, Rev. Sci. Instrum. **47**, 236 (1976).
[49]D. L. Eggleston, C. F. Driscoll, B. R. Beck, A. W. Hyatt, and J. H. Malmberg, Phys. Fluids B **4**, 3432 (1992).
[50]J. D. Jackson, *Classical Electrodynamics*, 2nd ed. (Wiley, New York, 1975).
[51]J. Tan and G. Gabrielse, Phys. Rev. Lett. **67**, 3090 (1991).
[52]J. Tan and G. Gabrielse, Phys. Rev. A **48**, 3105 (1993).
[53]C. S. Weimer, J. J. Bollinger, F. L. Moore, and D. J. Wineland, Phys. Rev. A **49**, 3842 (1994).

Downloaded 21 Jun 2001 to 132.239.73.116. Redistribution subject to AIP license or copyright, see http://ojps.aip.org/pop/popcr.jsp